Journal of
Applied Crystallography

ISSN 0021-8898

Received 16 August 2006
Accepted 16 March 2007

Evaluation of multiple small-angle neutron scattering including magnetic interactions

Jan Šaroun

Nuclear Physics Institute ASCR, v.v.i., 25068 Řež, Czech Republic, and Research Center Řež plc., Husinec-Řež 130, 25068, Czech Republic. Correspondence e-mail: saroun@ujf.cas.cz

Analytical formulae describing multiple small-angle neutron scattering in ferromagnetic materials are derived from transport equations. The derivation is based on Molière's theory of multiple small-angle scattering assuming that the mean free path of the neutrons is large compared to the size of the scatterers. In addition to the formalism developed earlier for nuclear scattering, the new formulation takes into account the spin dependence of the scattering cross section and spin flips caused by subsequent scattering events. This leads to an anomalous distribution of scattering intensity and polarization, as demonstrated by examples of model calculations and Monte Carlo simulations. In particular, multiple scattering of polarized neutrons can lead to either smoothing or sharpening of the scattered beam anisotropy depending on the polarization of the primary beam and the nuclear and magnetic contrasts of the scatterers. The presented theory has been implemented in the data-fitting program *SASProFit* suitable for both the modelling of multiple scattering effects and the analysis of experimental data.

1. Introduction

Multiple small-angle scattering (MSAS) leads, together with instrumental smearing, to partial loss of structural information contained in measured scattering curves. In many cases, this effect can be made negligible by measuring thin samples, using short neutron wavelengths or by dilution of the scatterers. However, there are situations when multiple scattering cannot be avoided, *e.g.* in high-resolution measurements focused on large inhomogeneities or in time-resolved experiments necessitating high count rates. In such cases, one has to take multiple scattering into account in the course of data analysis.

In the small-angle approximation, multiple scattering is described by Molière's theory, which can be derived from the transport equation for radiation particles passing through a scattering medium (Bethe, 1953). The theory is valid for any form of differential single-scattering cross section, provided that the scattering is limited to small angles and the mean free path of the particles is large compared to the size of the scatterers or, more generally, to the correlation length of the scattering medium. Schelten & Schmatz (1980) arrived at Molière's expressions using a multiconvolution approach, which turns out to be equivalent to Bethe's solution of the transport equation. They assumed the diffractive regime of neutron and X-ray scattering, in which scattering by a single particle is kinematical (described by the Born approximation). Their result was derived for azimuthally isotropic scattering functions, although Molière's theory also permits the treatment of anisotropic scattering or the calculation of scattering curves for infinite-slit geometry (Snyder & Scott, 1949). A full dynamical description of scattering by a spheroid particle has been used in the work of Berk & Hardman-Rhyne (1985, 1988) and Allen & Berk (1994) to calculate multiple scattering in the general case, including the refractive regime. This generalization permits the study of systems with large high-contrast inhomogeneities, such as microporous silica or plasma-sprayed ceramics coatings (Hardman-Rhyne & Berk, 1985; Hardman-Rhyne *et al.*, 1986; Long & Krueger, 1989; Allen *et al.*, 2002). Multiple magnetic scattering has been considered before in the calculations of polarized neutron beam transmission through ferromagnets (Halpern & Holstein, 1941; Hiismaki, 1983) and in the interpretation of critical scattering in ferromagnets (Toperverg *et al.*, 1979).

For a complete description of multiple scattering by magnetic inhomogeneities, one has to distinguish different components of the scattering cross section with respect to the initial and final spin states of the neutrons. In this work, Molière's theory is adapted so that the spin dependence of the scattering cross section as well as spin flips caused by subsequent scattering events are taken into account. In §2, the MSAS theory for nuclear scattering is reviewed in a form suitable for evaluation of two-dimensional anisotropic scattering curves and for further generalization to the case of magnetic scattering of polarized neutrons, which is introduced in §3. Examples of MSAS calculated for magnetic systems, particularly those showing anomalous intensity and polarization distributions due to multiple scattering, are presented and discussed in §4.

2. Nuclear multiple scattering

The formulae for MSAS of neutrons by nonmagnetic materials obtained by Schelten & Schmatz (1980) for isotropic systems can be expressed more generally in a vector form, which permits the inclusion of anisotropic scattering as well as an easy transition to the case of infinite-slit geometry. Let us start with the single-scattering differential cross section, $d\Sigma/d\Omega(\mathbf{q})$, which is related to the autocorrelation function of the medium by the pair of Fourier transformations

$$\frac{\mathrm{d}\Sigma}{\mathrm{d}\Omega}(\mathbf{q}) = \lambda^{-2}\int g(\mathbf{r})\cos(\mathbf{q}\cdot\mathbf{r})\ \mathrm{d}^2\mathbf{r}, \tag{1a}$$

$$g(\mathbf{r}) = k^{-2}\int \frac{\mathrm{d}\Sigma}{\mathrm{d}\Omega}(\mathbf{q})\cos(\mathbf{q}\cdot\mathbf{r})\ \mathrm{d}^2\mathbf{q}, \tag{1b}$$

where $k = 2\pi/\lambda$ is the magnitude of the neutron wavevector. Here we assume that, in the small-angle approximation of elastic scattering, the scattering vector $\mathbf{q}$ has only two components q_x and q_y in the detector plane, while $q_z = 0$. The function $g(\mathbf{r})$ is then the three-dimensional autocorrelation function of the medium, $\gamma(\mathbf{r}, z)$, projected along the beam axis (z),

$$g(\mathbf{r}) \equiv \lambda^2 \int_{-\infty}^{\infty} \gamma(\mathbf{r}, z)\ \mathrm{d}z. \tag{2}$$

The factor λ^2 and the square of the scattering contrast have been included in the definition of $g(\mathbf{r})$ in order to simplify following expressions. The total scattering cross section is then $\Sigma_\mathrm{T} = g(0)$, as follows from equation (1a) by integration over $\mathrm{d}\Omega = k^{-2}\,\mathrm{d}^2\mathbf{q}$. The beam profile $W(\mathbf{q}, t)$ as a function of apparent scattering vector $\mathbf{q}$ and depth in the sample t is given by the transport equation (Bethe, 1953)

$$\frac{\partial W(\mathbf{q}, t)}{\partial t} = k^{-2}\int W(\mathbf{q}', t)\frac{\mathrm{d}\Sigma}{\mathrm{d}\Omega}(\mathbf{q}-\mathbf{q}')\ \mathrm{d}\mathbf{q}' - \Sigma_\mathrm{T} W(\mathbf{q}, t). \tag{3}$$

Let us proceed from $W(\mathbf{q}, t)$ to its Fourier image,

$$H(\mathbf{r}, t) = k^{-2}\int W(\mathbf{q}, t)\cos(\mathbf{q}\cdot\mathbf{r})\ \mathrm{d}^2\mathbf{q}. \tag{4}$$

Equation (3) then transforms to

$$\frac{\partial H(\mathbf{r}, t)}{\partial t} = [g(\mathbf{r}) - g(0)]H(\mathbf{r}, t), \tag{5}$$

which for the boundary condition $W(\mathbf{q}, 0) = k^2\delta(\mathbf{q})$ has a simple solution,

$$H(\mathbf{r}, t) = \exp\big\{[g(\mathbf{r}) - g(0)]t\big\}. \tag{6}$$

It is easy to show that the solution for infinite-slit geometry, where the scattering is integrated along q_y/k, has the same form. One only needs to set $y = 0$ and replace $\mathbf{r}$ with the x coordinate in the equations (5) and (6).

3. Multiple scattering including magnetic interactions

When dealing with scattering of polarized neutrons by magnetic inhomogeneities, we need to distinguish four components of the scattering cross section for all the combinations of initial and final neutron spin states (Moon *et al.*, 1969),

$$\frac{\mathrm{d}\Sigma^{\pm\pm}}{\mathrm{d}\Omega}(\mathbf{q}) = S_\mathrm{N}(\mathbf{q}) + S_\mathrm{M}(\mathbf{q}) \mp S_\mathrm{NM}(\mathbf{q}), \tag{7a}$$

$$\frac{\mathrm{d}\Sigma^{\pm\mp}}{\mathrm{d}\Omega}(\mathbf{q}) = S_\mathrm{SF}(\mathbf{q}), \tag{7b}$$

where the indices N, M, NM and SF denote the nuclear, magnetic, nuclear–magnetic interference and spin-flip terms, respectively. Generally, there is also a spin-dependent spin-flip term which is zero for simple ferromagnets and therefore omitted in equation (7b). The partial cross sections $S_\mathrm{i}(\mathbf{q})$ (i = N, M, NM, SF) have to be calculated for a given microstructural model, which may include the simple model of aligned ferromagnetic particles in a nonmagnetic matrix considered later in this work as well as a more elaborated micromagnetics model (Weissmüller *et al.*, 2001; Löffler *et al.*, 2005). The particular form of the single-scattering cross section is irrelevant for the following considerations regarding multiple scattering. For each of the $S_\mathrm{i}(\mathbf{q})$ terms, equation (1b) defines the corresponding correlation function $g_\mathrm{i}(\mathbf{r})$ and the total scattering cross section $\Sigma_\mathrm{i} = g_\mathrm{i}(0)$. In addition, we have to introduce the total cross sections for absorption and large-angle scattering, Σ_A, and depolarization of the transmitted beam, Σ_D. The latter may include, for example, spin rotations in large ferromagnetic domains with misaligned magnetization, for which the scattering angle is negligibly small. On the other hand, the small-angle-scattering spin-flip cross section is already included in the term Σ_SF. In analogy to equation (5), we can now construct transport equations for neutron beams in the two spin states (+, −),

$$\frac{\partial H^+}{\partial t} = (g_\mathrm{N} + g_\mathrm{M} - g_\mathrm{NM})H^+ + g_\mathrm{SF}H^- - (\Sigma_\mathrm{T} - \Sigma_\mathrm{NM} + \Sigma_\mathrm{D})H^+ + \Sigma_\mathrm{D}H^-, \tag{8a}$$

$$\frac{\partial H^-}{\partial t} = (g_\mathrm{N} + g_\mathrm{M} + g_\mathrm{NM})H^- + g_\mathrm{SF}H^+ - (\Sigma_\mathrm{T} + \Sigma_\mathrm{NM} + \Sigma_\mathrm{D})H^- + \Sigma_\mathrm{D}H^+, \tag{8b}$$

where $\Sigma_\mathrm{T} = \Sigma_\mathrm{A} + \Sigma_\mathrm{N} + \Sigma_\mathrm{M} + \Sigma_\mathrm{SF}$. Note that the explicit notation of the independent variables $\mathbf{r}$ and t at the functions $H(\mathbf{r}, t)$ and $g_\mathrm{i}(\mathbf{r})$ is omitted. The first two terms on the right-hand side describe small-angle scattering for the given spin state as expressed by equations (7), while the other terms represent the attenuation of the neutron beam due to all kinds of scattering and absorption. This pair of equations actually describes a random walk of neutrons in given spin state through the scattering medium, where the mean free paths and $\mathbf{q}$-step distributions for the four spin transitions are given by Σ_i^{-1} and $S_\mathrm{i}(\mathbf{q})$ from equations (7). An analytical solution of these equations can thus be directly compared to Monte Carlo simulations of such a random walk, as we show later in this paper. For practical reasons, it is more convenient to solve the transport equations for $H \equiv H^+ + H^-$ and $P_\mathrm{f} \equiv H^+ - H^-$, which describe the total intensity as measured without polarization analysis and final polarization of the scattered neutron beam, respectively. Equations (8) then transform to

$$\frac{\partial H}{\partial t} = \big(g_\mathrm{N} + g_\mathrm{M} + g_\mathrm{SF}\big)H - g_\mathrm{NM}P_\mathrm{f} - \Sigma_\mathrm{T}H + \Sigma_\mathrm{NM}P_\mathrm{f}, \tag{9a}$$

$$\frac{\partial P_\mathrm{f}}{\partial t} = \big(g_\mathrm{N} + g_\mathrm{M} - g_\mathrm{SF}\big)P_\mathrm{f} - g_\mathrm{NM}H - (\Sigma_\mathrm{T} + 2\Sigma_\mathrm{D})P_\mathrm{f} + \Sigma_\mathrm{NM}H. \tag{9b}$$

At the sample entry surface, we assume $W(\mathbf{q}) = k^2\delta(\mathbf{q})$ and polarization P_i, hence the boundary condition is $H = 1$ and $P_\mathrm{f} = P_\mathrm{i}$ for $t = 0$. Equations (9) then have a solution in the form

$$H = \exp(\alpha t)\big\{\cosh(\beta t) + \beta^{-1}\big[g_\mathrm{SF} + \Sigma_\mathrm{D} - P_\mathrm{i}(g_\mathrm{NM} - \Sigma_\mathrm{NM})\big]\sinh(\beta t)\big\} \tag{10a}$$

$$P_\mathrm{f} = \exp(\alpha t)\big\{P_\mathrm{i}\cosh(\beta t) - \beta^{-1}\big[g_\mathrm{NM} - \Sigma_\mathrm{NM} + P_\mathrm{i}\big(g_\mathrm{SF} + \Sigma_\mathrm{D}\big)\big]\sinh(\beta t)\big\}, \tag{10b}$$

where $\alpha \equiv g_\mathrm{N} + g_\mathrm{M} - \Sigma_\mathrm{T} - \Sigma_\mathrm{D}$ and $\beta \equiv [(g_\mathrm{NM} - \Sigma_\mathrm{NM})^2 + (g_\mathrm{SF} + \Sigma_\mathrm{D})^2]^{1/2}$.

It is usually possible to calculate the nuclear component of the correlation function, $g_\mathrm{N}(\mathbf{r})$ directly from a real-space model represented by the nuclear scattering length density, $\rho_\mathrm{N}(\mathbf{r})$. On the other hand, the magnetic components have to include the $\mathbf{q}$-dependence of the scattering amplitude in the form of the Halpern–Johnson vector,

$$\mathbf{M}^\perp(\mathbf{q}) = |\mathbf{q}|^{-2}\mathbf{q}\times[\boldsymbol{\mu}(\mathbf{q})\times\mathbf{q}], \tag{11}$$

where $\boldsymbol{\mu}(\mathbf{q})$ is the Fourier image of the magnetization. A prescription for the calculation of the beam distribution, $W(\mathbf{q}, t)$, therefore involves calculation of single-scattering cross sections for the given structural model, then the correlation functions $g_\mathrm{i}(\mathbf{r})$ are obtained by

the Fourier transformation [equation (1*b*)] and converted to $H(\mathbf{r}, t)$ using equations (10). Finally, $W(\mathbf{q}, t)$ is calculated by the inverse of the Fourier transformation [equation (4)]. A similar procedure can be used for the $\mathbf{q}$-dependence of the final polarization.

By definition, the functions $H(\mathbf{r}, t)$ and $W(\mathbf{q}, t)$ also contain the transmitted (unscattered) part of the beam. The intensity and polarization of the transmitted beam can therefore be calculated from equations (10) by setting $g_i = 0$ (or equivalently $r = \infty$), so that $\beta \equiv (\Sigma_{NM}^2 + \Sigma_D^2)^{1/2}$ and

$$H(\infty, t) = \exp\left[-(\Sigma_T + \Sigma_D)t\right] \times \left[\cosh(\beta t) + \beta^{-1}(\Sigma_D + P_i\Sigma_{NM})\sinh(\beta t)\right] \quad (12a)$$

$$P_f(\infty, t) = \exp\left[-(\Sigma_T + \Sigma_D)t\right] \times \left[P_i\cosh(\beta t) + \beta^{-1}(\Sigma_{NM} - P_i\Sigma_D)\sinh(\beta t)\right]. \quad (12b)$$

This is actually identical with the result obtained by Halpern & Holstein (1941) for transmission of neutrons through an incompletely saturated polycrystalline ferromagnet.

As a special case, let us consider purely magnetic scattering, for which $g_{NM} = 0$, and equation (10*a*) yields

$$H = \exp[(\alpha + \beta)t]. \quad (13)$$

We may see that, without the nuclear–magnetic interference term, there is no substantial difference in the treatment of multiple scattering with respect to the result obtained by Schelten & Schmatz (1980). Obviously, it is the nuclear–magnetic interference term which is responsible for partial polarization of the scattered neutron beam and may lead, in combination with multiple scattering, to an anomalous shape of scattered beam profiles. This is demonstrated with several examples of model calculations in the following section.

4. Model calculations

The following model calculations are based on a simple structural model consisting of spherical ferromagnetic particles embedded in a nonmagnetic matrix with a log-normal distribution of sphere radii,

$$\frac{\mathrm{d}f(R)}{\mathrm{d}R} = \frac{f_0}{(2\pi)^{1/2}\sigma R}\exp\left\{-0.5\sigma^{-2}\left[\ln(R) - \ln(R_0) + 0.5\sigma^2\right]^2\right\}, \quad (14)$$

characterized by the total volume fraction, f_0, mean radius, R_0 and distribution width, σ. We assume perfect alignment of the particles magnetization in an external magnetic field oriented perpendicularly to the neutron beam, along the x axis. In such a case, the partial scattering cross sections entering in equations (7) can be expressed in polar coordinates as

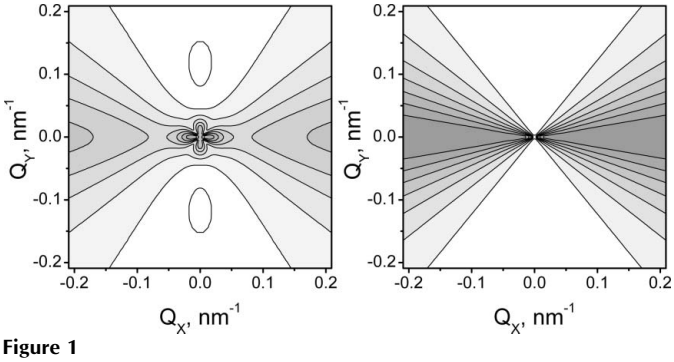

Figure 1
Polarization of scattered neutrons for (a) multiple scattering (p = 0.77) and (b) single scattering (p = 0.05). The initial beam was unpolarized.

$$S_i(q, \varphi) = a_i(\varphi)F(q)^2, \quad (15)$$

where $q = |\mathbf{q}|$ and $F(q)^2$ is the square of the particle form factor averaged over the size distribution. In the small-angle approximation, the factors $a_i(\varphi)$ are

$$a_N = \rho_N^2, \qquad a_M(\varphi) = \rho_M^2\sin(\varphi)^4,$$
$$a_{NM}(\varphi) = 2\rho_N\rho_M\sin(\varphi)^2, \quad a_{SF}(\varphi) = \rho_M^2\sin(\varphi)^2\cos(\varphi)^2, \quad (16)$$

where φ is the angle between the magnetization and scattering vectors and ρ_N and ρ_M are the nuclear and magnetic scattering length contrasts, respectively. The calculations were made on a grid of 128 × 128 pixels with the help of the data-fitting program *SASProFit* (Saroun, 2000, http://omega.ujf.cas.cz/SAS), which implements the above formalism together with other tools for SAS data analysis. We neglect instrumental smearing and interparticle interference in order to assess the multiple scattering effects only. However, the structure factor can be included in $S_i(\mathbf{q})$ when necessary, thus allowing the study of dense correlated systems. Appropriate instrumental smearing can be applied to $W(\mathbf{q}, t)$ in the usual way.

4.1. Polarization of the scattered beam

In the first example, polarization of the scattered beam was calculated in the single and multiple scattering regimes with total scattering probabilities p = 0.05 and 0.77, respectively, adjusted by the corresponding volume fractions of the spheres. The values of the model parameters were: $\rho_M = 4.97 \times 10^{10}$ cm^{-2}, $\rho_N/\rho_M = 0.5$, R_0 = 100 nm and $\sigma = 0.3$. The volume fraction and sample thickness were adjusted to yield the scattering probabilities given above. The results for an unpolarized initial beam (Fig. 1) show that multiple scattering introduces significant dependence of polarization on the magnitude of the scattering vector, while in the single-scattering case the polarization depends only on the azimuth angle as $\sin(\varphi)^2$.

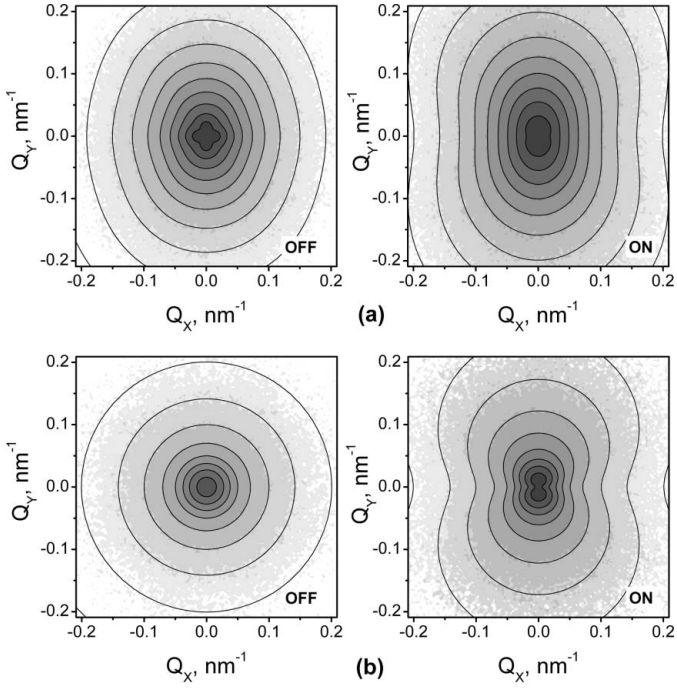

Figure 2
Analytical calculations (lines) and Monte Carlo simulations (gray-scale maps) of the scattering intensity, assuming a perfectly polarized incident beam with spin-flipper switched either OFF (left, $P_i = 1$) or ON (right, $P_i = -1$). Multiple scattering with scattering probability p = 0.77 (a) is compared to the single scattering case (b).

4.2. Distribution of scattering intensity, comparison with Monte Carlo simulations

In the next example, we have calculated multiple scattering for the same model as in the previous case, assuming an ideally polarized initial beam with $P_i = 1$ (spin flipper off) or $P_i = -1$ (flipper on). The ratio $\rho_N/\rho_M = 0.5$ was selected because it yields azimuthally isotropic single scattering for $P_i = 1$ and the effect of spin transitions in the multiple scattering process is clearly revealed (see Fig. 2). As mentioned above, the transport equations (8) describe a random walk accompanied by the exchange between spin states of neutrons passing through the sample. Such a random walk process was simulated by the Monte Carlo method using the model single-scattering cross section as the distribution function for walk steps in **q** and t. The result is compared with the analytically calculated beam profiles in Fig. 2. This example clearly demonstrates that multiple scattering changes the $\sin(\varphi)^2$ modulation expected for single scattering to a more complex one with fourfold symmetry at small **q**. Obviously, this effect arises from the difference between scattering cross sections for the two spin states due to the nuclear–magnetic interference term. After the first scattering event, the initially polarized beam ($P_i = 1$) is partly depolarized by spin-flip scattering with $\sin(2\varphi)^2$ dependence. Neutrons with their spin flipped to the (−) state undergo secondary scattering with higher probability compared to those in the (+) state. Consequently, the (−) neutrons are partly removed from the central part of the neutron beam, leaving there an 'imprint' modulated as $\sin(2\varphi)^2$ (see Fig. 3). Multiple scattering may thus lead either to smoothing or sharpening of the scattered beam anisotropy, depending on the polarization of the primary beam and the ratio of the magnetic and nuclear scattering contrasts.

In any case, multiple scattering changes the φ dependence of the scattered beam distribution and the methods commonly used to separate magnetic and nuclear scattering components may become inappropriate. The next example illustrates this problem on the evaluation of ρ_M/ρ_N from the flipping ratio.

4.3. Flipping ratio

The last example uses similar model parameters as the previous ones, but the scattering contrast and size range were set to approach a real system of magnetite particles in glassy ceramics studied earlier by Lembke *et al.* (1999). The corresponding model parameters were thus $\rho_M = 1.36 \times 10^{10}$ cm^{-2}, $\rho_N/\rho_M = 1.6$, $R_0 = 10$ nm, $\sigma = 0.3$ and $f = 20\%$. The sample thickness was set to 0.2, 1 and 5 mm resulting in the scattering probabilities of 1.8, 9 and 37%, respectively, at $P_i = -1$. Scattering curves were calculated for two detector distances, 1 and 4 m, in order to cover a broader **q** range and to reduce the smearing effect near the beam center caused by the finite pixel size. From the scattering curves obtained for the two final spin states, $W^{\pm}(\mathbf{q})$, the ratio ρ_M/ρ_N was calculated as (Wiedenmann, 2000)

$$\frac{\rho_M}{\rho_N}(q) = \frac{1}{2}\frac{W^-(q_\perp) - W^+(q_\perp)}{W^-(q_{||}) + W^+(q_{||})}, \qquad (17)$$

where $q_\perp$ and $q_{||}$ are the q values measured along the directions perpendicular and parallel to the applied magnetic field, respectively.

The ratio ρ_M/ρ_N should be constant for our simple model. However, multiple scattering causes an apparent q dependence as shown in Fig. 4. Consequently, multiple scattering may lead to a significant bias of structural parameters evaluated from SANS measurements with polarized neutrons even for a moderate scattering probability of $p \simeq 10\%$. Unfortunately, the q dependence of the ρ_M/ρ_N ratio shown in Fig. 4 is not a characteristic feature of multiple scattering, since a very similar effect can also be observed in the single-scattering regime, *e.g.* for a core–shell model of magnetic particles with varying magnetic and nuclear contrasts (Wiedenmann, 2000).

5. Concluding remarks

The main result of this work is represented by the pair of equations (10), which permit the calculation of the intensity and polarization of multiple small-angle scattering by magnetic and nuclear inhomogeneities. They are valid under the same conditions as Molière's theory of multiple scattering, *i.e.* the neutrons' mean free path has to be large compared to the sizes of the inhomogeneities. Both analytical calculations and Monte Carlo simulations predict anomalous modulation of the scattering at small q with respect to the angle φ between magnetization and scattering vector in the case when the nuclear–magnetic interference part of the scattering cross section can not be neglected. Generally, multiple scattering changes the anisotropy of the scattered beam intensity and polarization. Care should therefore be taken when employing the $\sin(\varphi)^2$ dependence of magnetic scattering in data analysis, unless multiple scattering can *a priori* be ruled out. While multiple scattering can probably be avoided when studying small nanoparticles like in ferrofluids, its significance increases rapidly with the size of the inhomogeneities studied. The results presented here might therefore be useful for analyzing experimental data on composite materials containing ferromagnetic grains or ferromagnets with coarse nonmagnetic

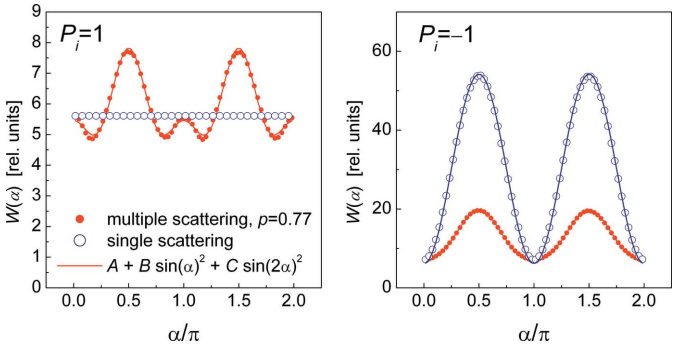

Figure 3
Profiles of a neutron beam scattered at $q = 0.038$ nm^{-1} corresponding to the two-dimensional patterns shown in Fig. 2, normalized to $W = 1$ at $\varphi = 0$. The profiles were fitted to the function $W(\varphi) = A + B\sin(\varphi)^2 + C\sin(2\varphi)^2$ (lines).

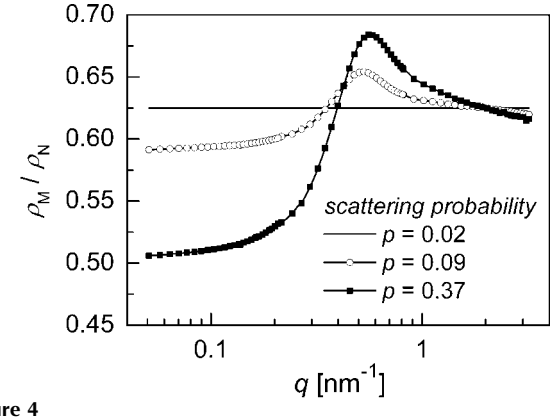

Figure 4
The apparent ratio of the magnetic and nuclear scattering contrast evaluated from the calculated MSAS curves with polarized neutrons.

precipitates or pores. Equations (10) may then serve as a theoretical basis for two-dimensional data analysis involving multiple scattering corrections. They have been implemented in the data-fitting program *SASProFit* (Saroun, 2000), which permits both the calculation of model scattering curves including multiple scattering and data fitting.

This research was supported by the Institutional Research Plan AV0Z10480505 and by the project MSM2672244501.

References

Allen, A. J. & Berk, N. F. (1994). *J. Appl. Cryst.* **27**, 878–891.
Allen, A. J., Berk, N. F., Ilavsky, J. & Long, G. G. (2002). *Appl. Phys. A*, **74** (Suppl.), S937–S939.
Berk, N. F. & Hardman-Rhyne, K. A. (1985). *J. Appl. Cryst.* **18**, 467–472.
Berk, N. F. & Hardman-Rhyne, K. A. (1988). *J. Appl. Cryst.* **21**, 645–651.
Bethe, H. A. (1953). *Phys. Rev.* **89**, 1256–1266.
Halpern, O. & Holstein, T. (1941). *Phys. Rev.* **59**, 960–981.
Hardman-Rhyne, K. A. & Berk, N. F. (1985). *J. Appl. Cryst.* **18**, 473–479.
Hardman-Rhyne, K. A., Frase, K. G. & Berk, N. F. (1986). *Physica B*, **136**, 223–225.
Hiismaki, P. (1983). *J. Phys. D Appl. Phys.* **16**, 2405–2413.
Lembke, U., Hoell, A., Kranold, R., Müller, R., Schüppel, W., Goerigk, G., Gilles, R. & Wiedenmann, A. (1999). *J. Appl. Phys.* **85**, 2279–2286.
Löffler, J. F., Braun, H. B., Wagner, W., Kostorz, G. & Wiedenmann, A. (2005). *Phys. Rev. B*, **71**, 134410.
Long, G. G. & Krueger, S. (1989). *J. Appl. Cryst.* **22**, 539–545.
Moon, R. M., Riste, T. & Koehler, W. C. (1969). *Phys. Rev.* **181**, 920–931.
Saroun, J. (2000). *J. Appl. Cryst.* **33**, 824–828.
Schelten, J. & Schmatz, W. J. (1980). *J. Appl. Cryst.* **13**, 385–390.
Snyder, H. S. & Scott, W. T. (1949). *Phys. Rev.* **76**, 220–225.
Toperverg, B. P., Runov, V. V., Gukasov, A. G. & Okorokov, A. I. (1979). *Phys. Lett. A*, **71**, 289–291.
Weissmüller, J., Michels, A., Barker, J. G., Wiedenmann, A., Erb, U. & Shull, R. D. (2001). *Phys. Rev. B*, **63**, 214414.
Wiedenmann, A. (2000). *J. Appl. Cryst.* **33**, 428–432.